



Individual synaptic vesicles mediate stimulated exocytosis from cochlear inner hair cells

Chad Paul Grabner^{a,b,1} and Tobias Moser^{a,b,c}

^aSynaptic Nanophysiology Group, Max Planck Institute for Biophysical Chemistry, 37077 Göttingen, Germany; ^bInstitute for Auditory Neuroscience and InnerEarLab, University Medical Center Göttingen, 37075 Göttingen, Germany; and ^cAuditory Neuroscience Group, Max Planck Institute for Experimental Medicine, 37075 Göttingen, Germany

Edited by A. J. Hudspeth, The Rockefeller University, New York, NY, and approved October 19, 2018 (received for review July 9, 2018)

Spontaneous excitatory postsynaptic currents (sEPSCs) measured from the first synapse in the mammalian auditory pathway reach a large mean amplitude with a high level of variance (CV between 0.3 and 1). This has led some to propose that each inner hair cell (IHC) ribbon-type active zone (AZ), on average, releases ~6 synaptic vesicles (SVs) per sEPSC in a coordinated manner. If true, then the predicted change in membrane capacitance (C_m) for such multivesicular fusion events would equate to ~300 attofarads (aF). Here, we performed cell-attached C_m measurements to directly examine the size of fusion events at the basolateral membrane of IHCs where the AZs are located. The frequency of events depended on the membrane potential and the expression of $Ca_v1.3$, the principal Ca^{2+} -channel type of IHCs. Fusion events averaged 40 aF, which equates to a normal-sized SV with an estimated diameter of 37 nm. The calculated SV volumes showed a high degree of variance ($CV > 0.6$). These results indicate that SVs fused individually with the plasma membrane during spontaneous and evoked release and SV volume may contribute more variability in EPSC amplitude than previously assumed.

ribbon synapse | synaptic efficiency | multivesicular release | univesicular release | membrane capacitance

Sound information is transmitted from inner hair cells (IHCs) in the cochlea to the brain via spiral ganglion neurons (SGNs). These bipolar neurons receive excitatory input from IHCs and signal this information directly to the auditory brainstem as discrete action potentials (APs). Several studies have documented that the rate of spontaneous excitatory postsynaptic currents (sEPSCs) and evoked EPSCs (eEPSCs) depends on Ca^{2+} -stimulated release of glutamate from IHCs (1–4). Modeling and experimental work indicates that the majority of these EPSCs can trigger an SGN AP (5). What remains less clear is how many synaptic vesicles (SVs) give rise to s/eEPSC and, so, to an AP.

The standard approach used to estimate the postsynaptic response to a single SV release event entails measuring postsynaptic currents (PSCs) under conditions of low release probability, e.g., by blocking presynaptic APs with tetrodotoxin. These miniature PSCs (mPSCs) are typically equated to the independent fusion of SVs. mPSC amplitude is widely reported to be insensitive to changes in extracellular Ca^{2+} , and this holds true even when the frequency of spontaneous mPSCs is steeply enhanced by elevating extracellular Ca^{2+} levels (6, 7). In contrast, a PSC evoked by an AP often increases in amplitude as extracellular Ca^{2+} levels are elevated, which is widely interpreted as multiple SVs fusing in unison to create the evoked PSC (ref. 7; for review, see ref. 8). Whether this is multivesicular release per synapse (MVR, i.e., more than 1 SV release per AP) or recruitment of more synapses that support univesicular release (UVR) depends on the system at hand.

While not driven by APs, mammalian IHCs follow this general description in that (i) the eEPSC at the onset of a presynaptic depolarization is often larger than the sEPSCs and (ii) the mean sEPSC size is relatively constant during changes in event frequency and changes in extracellular Ca^{2+} levels (9, 10). Since

each afferent SGN is thought to contact one ribbon-type AZ, where ~10–30 SVs are thought to be in fusion competent states (11, 12), multiple SVs can be released per AZ even upon brief presynaptic depolarizations. However, there is controversy surrounding whether sEPSCs and the eEPSC observed during sustained presynaptic stimulation result from the fusion of a single SV (UVR) or from coordinated multivesicular release (cMVR). The original description concluded that cMVR of 4–8 SVs mediates IHC release events (3). A more recent study, derived from postsynaptic SGN recordings and mathematical modeling of the IHC ribbon synapse, concluded that UVR might govern IHC release events (9). Clearly, further work is required to elucidate the nature of exocytosis from mammalian IHCs.

Here, we made cell-attached membrane capacitance (C_m) recordings of exocytosis from mouse IHCs, thereby avoiding many of the complications associated with the interpretation of postsynaptic recordings. Cell-attached C_m recordings have been made from various secretory cells and proven useful in resolving a wide range of vesicle sizes, from single SVs (13) to secretory granules (14), and within the same recording (15). This approach has also been utilized to distinguish between UVR and a form of MVR called compound exocytosis (13, 16, 17). Here, we take an approach that involves stimulating the membrane patch directly and show that SV fusion in IHCs is voltage-dependent and requires Ca^{2+} entry through $Ca_v1.3$ channels. The stimulated fusion events have an equivalent SV diameter of 37 nm, close to that measured with electron microscopy, and the shape of the

Significance

Synaptic transmission is codetermined by presynaptic and postsynaptic neurons. Therefore, to understand how the inner hair cell (IHC) signals to spiral ganglion neurons at the first synapse in the auditory pathway, here we directly studied individual membrane fusion events by making cell-attached membrane capacitance recordings from IHCs, for which the quantal size is debated. The observed fusion steps in membrane capacitance are consistent with the quantal hypothesis of synaptic transmission in which individual synaptic vesicles undergo exocytosis independently from each other. This finding, in conjunction with previous work, raises the exciting possibility that action potential generation can be triggered by the release of a single vesicle at the IHC synapse.

Author contributions: C.P.G. and T.M. designed research; C.P.G. performed research; C.P.G. contributed new reagents/analytic tools; C.P.G. analyzed data; and C.P.G. and T.M. wrote the paper.

The authors declare no conflict of interest.

This article is a PNAS Direct Submission.

This open access article is distributed under [Creative Commons Attribution License 4.0 \(CC BY\)](https://creativecommons.org/licenses/by/4.0/).

¹To whom correspondence should be addressed. Email: chadgrabner@gmail.com.

This article contains supporting information online at www.pnas.org/lookup/suppl/doi:10.1073/pnas.1811814115/-DCSupplemental.

Published online November 21, 2018.

size distribution follows that expected for UVR. The estimated variance in SV volume was large ($CV > 0.6$). The findings suggest that mammalian IHC are not prone to cMVR during spontaneous and sustained exocytosis as suggested (3, 16), but rather release may be dominated by a UVR scheme. In essence, this may create a uniquely sensitive, highly efficient synaptic transfer of 1 SV for 1 AP. This signaling regime will protect the AZ from fatigue and allow high frequency signaling.

Results

Step-Like Full-Fusion Events Predominate. For cell-attached C_m recordings, we targeted the pipette to the basolateral membrane at the modiolar face of IHCs in the apical turn of the cochlea taken from hearing mice (4–8 wk old). The basolateral portion of the IHC has the highest density of ribbons, as this is where the SGNs contact the IHC (18). The SGN dendrites were dislodged from the IHC with positive pipette pressure to free the pre-synaptic membrane. The thick wall patch pipettes used here had a series resistance of ~ 2.5 M Ω , which is expected to have a $5 \mu\text{m}^2$ area of free membrane at the dome of the patch (13, 19). Given the large number of synapses (~ 12 synapses per IHC at the tonotopic position of recording; ref. 18) with a mean nearest neighbor distance of $2 \mu\text{m}$ (18), we estimated that the large recording patches made from the basolateral pole of the IHC would have a fair chance of capturing an AZ. Finally, to achieve an optimal C_m signal-to-noise ratio, we used the hardware-based Lock-in amplifier method (20), and applied sinewave settings similar to those employed to monitor small vesicles ~ 45 nm in diameter (13, 15).

The exemplar traces presented in Fig. 1A show a series of step-like jumps in C_m measured from a wild-type IHC. Neither the corresponding conductance nor membrane current traces showed transitions that correlated with the steps in C_m . This indicates the Lock-in signals were well separated from one another (further described in *SI Appendix, Figs. S1 and S2*). These simple up steps in C_m without subsequent down steps are referred to as “full-fusion” events (13). As reported here for IHCs, and in many other preparations (13–15, 21), full fusion was the most common type of event. Of nine cells, six exhibited only full-

fusion events, and from the remaining three cells, 92% of the events were full fusion (185/201 events, from three patches). The other 8% of the fusion events were followed by a decline in C_m that was slower than the preceding C_m up step (rising and falling phase time constants: 3.3 ± 0.7 ms and 66.3 ± 18.2 ms, respectively; $P = 0.002$, $n = 16$) (*SI Appendix, Fig. S3 A–D*). These infrequent, peculiar events likely resembled “pseudo-flicker” fusion (22), and they differ from transient fusion events that are often called “kiss-and-run” and characterized as having a fast rise in C_m and a similarly fast fall in C_m (21, 23). In some situations, such as pituitary lactotrophs, a high percentage of the fusion events are kiss-and-run (24), and certain perturbations can increase the frequency of kiss-and-run events (24, 25).

The Real component of the Lock-in signal is an aggregate of conductances. In some instances, changes in membrane current (I_m) were clearly reflected in the G trace, which we designate as changes in membrane conductance (G_m) (*SI Appendix, Fig. S1*). Another signal potentially carried in the G trace can be related to a fusion pore conductance (G_{pore}), which arises when a resistive pore forms between the vesicle and plasma membrane (for review, ref. 26). After inspection of traces with and without smoothing (as in Fig. 1A and B), a G_{pore} signal could not be found (*SI Appendix, Signal Processing and Fig. S2*). Other studies have reported that small vesicle full-fusion events are not (15), or rarely accompanied by a G_{pore} signal (1.4% of events; ref. 13). Since the G_{pore} signal is directly proportional to vesicle size (27, 28), it has been studied extensively for large granules that are 200–1,000 nm in diameter and yielded large fusion events (C_m steps > 1 fF) (for review, ref. 26). In contrast, IHCs have the smallest SVs (~ 36 nm) to be evaluated to date with the on-cell C_m method; thus, the G_{pore} signal may be too small to detect as a previous analysis predicted (29).

Fusion Is Dependent on Voltage-Dependent Calcium Channels. Previously, researchers elevated extracellular KCl to depolarize the cell and stimulate vesicle fusion, because direct voltage stimulation of patches via the patch pipette rarely evoked fusion (13–15, 21). In contrast, we find that the event frequency in membrane patches of wild-type IHCs is sensitive to voltage changes applied to the patch pipette relative to the ground electrode. At the resting membrane voltage (V_{rest}), the event frequency was 0.22 ± 0.04 Hz ($n = 8$ cells) (V_{rest} assumed to be -55 mV; ref. 30). When the patches were hyperpolarized by 20 mV (to V_m : -75 mV, Fig. 2A and C), there was a consistent suppression of event frequency (0.01 ± 0.01 Hz; 22-fold decrease from V_{rest} with $P = 0.001$; $n = 5$). When the patches were depolarized by 20 mV (to V_m : -35 mV, Fig. 2B), the event frequency increased by twofold above V_{rest} (0.45 ± 0.1 Hz; significant increase from rest, $P = 0.044$; $n = 7$). The dependence of event frequency on V_m is summarized in Fig. 3A. The stimulated event frequency reported here is similar to what others reported when using KCl (13, 15) or other secretagogues (31) to initiate fusion in preparations studied with the on-cell configuration.

Given that the loss of $\text{Ca}_v1.3$ from IHCs [via disruption of the $\text{Ca}_v1.3\alpha_1$ gene: $\text{Ca}_v1.3$ knockout (ko)] leads to $>90\%$ reduction in whole-cell calcium current (4) (see also Fig. 3B), and a dramatic impairment in exocytosis as judged by whole-cell C_m recordings (32), IHCs from $\text{Ca}_v1.3$ ko mice were studied to address whether $\text{Ca}_v1.3$ supports stimulated SV fusion in the on-cell configuration. Fig. 2D–F shows recordings from a $\text{Ca}_v1.3$ ko IHC that was silent at V_{rest} and when depolarized. On average, the frequency of fusion was not significantly altered when patches from $\text{Ca}_v1.3$ ko IHCs were held at rest V_m : -55 mV (0.07 ± 0.04 Hz; $n = 5$) versus depolarized to V_m : -35 mV (0.05 ± 0.04 Hz; $P = 0.75$, $n = 4$). The event frequencies measured from wild-type IHCs held at V_m : -55 mV and -35 mV were 4- and 11-fold higher, respectively, than what was observed for $\text{Ca}_v1.3$ ko IHCs held at

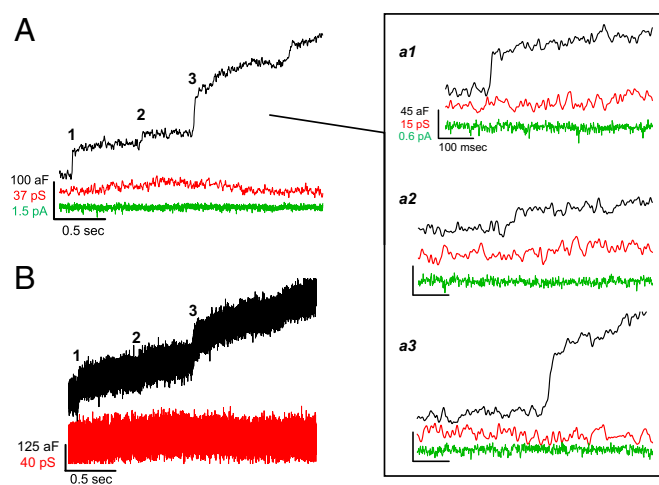


Fig. 1. Full-fusion events are the most common. (A) Recording from a wild-type IHC that shows a staircase of up steps in C_m (black trace), which appear to lack correlated changes in conductance (red trace) or membrane current (green trace). (a1–a3) Magnified view of fusion events from A (individual steps a1–a3 presented at same scale as in a1). (B) Same traces as in A (C_m and G), but not smoothed to reveal potential transient G signals associated with C_m fusion events. Lock-in sinewave settings: frequency, 58.5 kHz; V_{rms} , 200 mV.

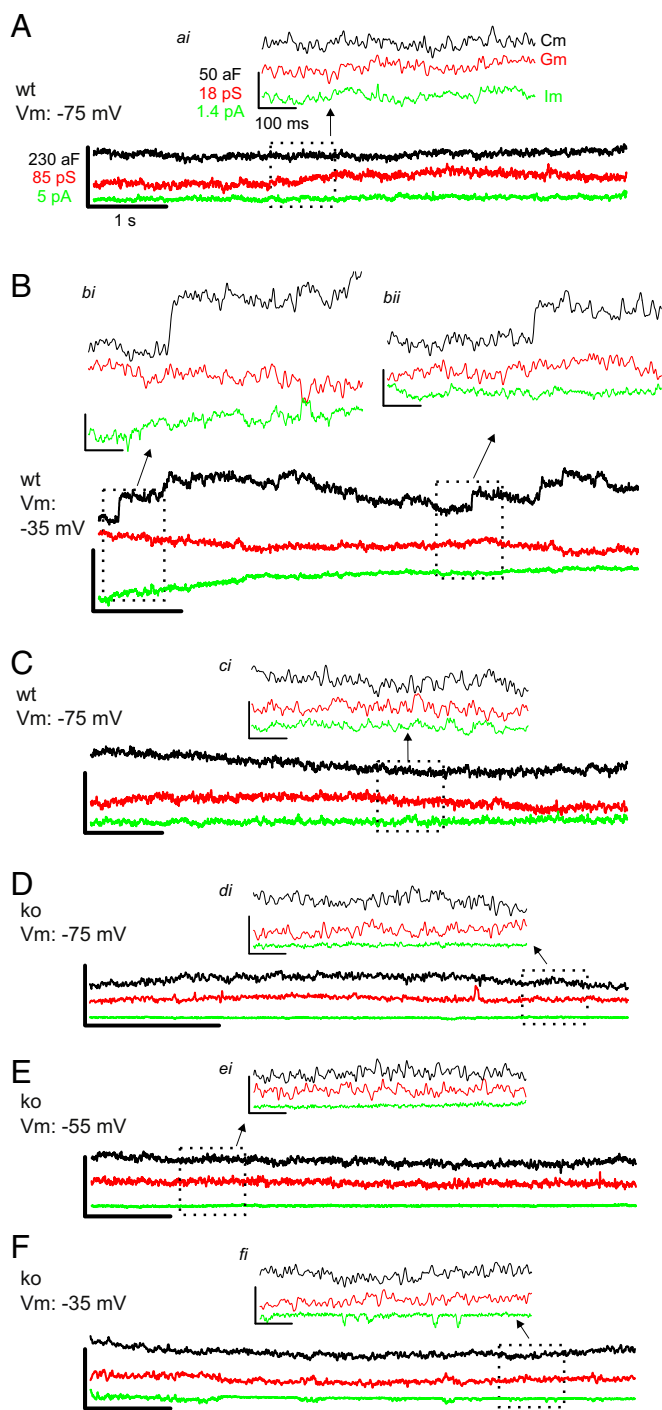


Fig. 2. Example responses measured from wild-type (wt) and $Ca_v1.3$ -ko IHCs given depolarizing steps. (A–C) Chronology of on-cell recordings made from a wild-type cell with the patch V_m varied from -75 mV (A) to -35 mV (B), and back to -75 mV (C). (Insets *ai* and *ci*) Zoomed views illustrate a lack of fusion events at $V_m = -75$ mV. (B) Patch at $V_m = -35$ mV exhibits fusion events observed as upward steps in C_m without mirrored changes in membrane conductance (G_m) or membrane current (I_m). Two example fusion events are presented in *bi* and *bii*. (D–F) On-cell recordings made from an individual $Ca_v1.3$ -ko IHC patch held at $V_m = -75$ mV (D); $V_m = -55$ mV (E); $V_m = -35$ mV (F). Traces have the same scale bar values as in A, and the *Insets* are scaled to the values as shown in *ai*. Lock-in sinewave settings: frequency, 58.5 kHz; V_{rms} , 150 mV.

the same V_m values (sig. diff. $P < 0.008$; Fig. 3A). The results suggest that coupling of the voltage stimulus to SV fusion is mediated by $Ca_v1.3$ in the on-cell configuration, lending further

support to the specificity of the C_m events as reporting Ca^{2+} -triggered SV fusion.

Fusion Event Amplitude Follows a Normal Vesicle Size Distribution.

To estimate the amplitude of fusion events, patches with low noise levels were analyzed [~ 4 attofarads (aF) rms noise]. An overlay of fusion events measured from an individual wild-type IHC highlights the variability in step height (Fig. 4A; only one patch recorded per cell). The distribution of event amplitudes measured from this cell peaked around 40 aF and was skewed toward larger sizes (Fig. 4B). Likewise, the plot of 416 events acquired from seven wild-type cells peaked around 40 aF and skewed rightward (Fig. 4C and D). Only 1.9% (8/416) of the events were >200 aF, 6.3% (26/416 events) were >100 aF, and the majority of events, 69% (285/416), were <50 aF (Fig. 4C). The average fusion event was 40.2 ± 3.3 aF (mean \pm SE; $n = 7$ patches), and this was made by averaging the median step amplitude derived from each cell (on average 59 events per patch; range: 29–99 events per patch). By using a specific capacitance of 9.1 fF/ μm^2 and assuming a spherical vesicle geometry (21), the equivalent SV diameters were calculated for the different size ranges. Only 1.9% of the events are estimated to be >83.6 nm (200 aF), 6.3% are >59.1 nm (100 aF), the majority (69%) are <41.8 nm (50 aF) (Fig. 4E), and the mean diameter calculated from the median per cell was 37.3 ± 1.1 nm (mean \pm SE). Making a grand average over 93.7% of all equivalent vesicle diameters, those <59.1 nm, gave a value of 37.3 ± 7.8 nm (mean \pm SD; 390 events, $n = 7$ cells), and a coefficient of variation (SD/mean) = 0.21. The resulting plot of diameters when fit with a Gaussian function (solid line, Fig. 4E) gave a distribution centered at 36.2 nm and a SD = 9.3 nm (CV = 0.26), which is in good agreement with the grand average, and indicates that the event amplitudes are normally distributed. These estimates closely approximate electron microscopy results that report normally distributed SV diameters with a mean value of 36.9 nm and a CV = 0.20 (33) (dashed line in Fig. 4E). However, conversion of C_m step values into equivalent SV volumes, which should be proportional to transmitter content of a SV (34–36), yields a distribution that is highly skewed (Fig. 4F), with a CV = 1.57 when calculated from all events ($5.53 \times 10^{-20}/3.52 \times 10^{-20}$ L). Using steps <100 aF gives a CV = 0.65 ($1.61 \times 10^{-20}/2.48 \times 10^{-20}$ L). Published CVs for EPSC measured from mammalian IHCs range from 0.3 to 1 (3, 9, 37, 38), and the estimated variance in SV volume falls within this range.

Stimulation Conditions Did Not Alter the Event Amplitude Distribution. It is known that stimulation conditions (9, 16, 25, 39) and genetic manipulations (16, 40) can influence quantal release properties (for

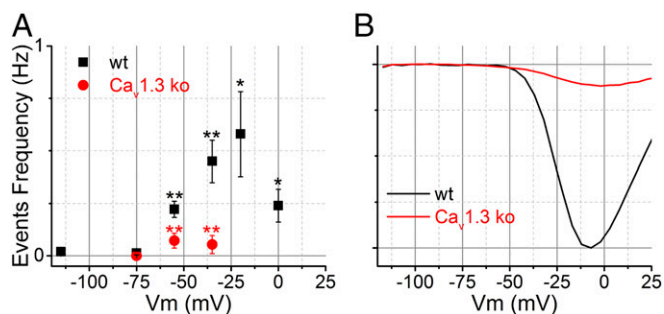


Fig. 3. Summary of fusion event frequency for wild-type (wt) and $Ca_v1.3$ -ko IHCs. (A) Plot of event frequency for wild-type ($n = 8$ at rest, and $n = 7$ depolarized) and $Ca_v1.3$ -ko IHCs at different V_m ($n = 5$). (B) Normalized I_{Ca} for wild-type and $Ca_v1.3$ -ko IHCs taken from Brandt et al. (32). Black asterisks indicate statistical comparison between wild type at rest ($V_m = -75$ mV) versus at depolarized V_m values, and red asterisks compare wild type and ko at the same V_m ($*P < 0.05$ and $**P < 0.01$).

Table 1. Average fusion event properties

Ca _v 1.3 genotype	Step amplitude, aF	
	Wild type	Ko
Rest	43.0 ± 4.0	40.4 ± 2.9
Depolarized	38.5 ± 3.6	36.0 ± 6.2
Rest + Depolarized	40.2 ± 3.3	41.3 ± 3.9

Values are presented as mean ± SE and calculated from the median step size per stimulation condition, across five knockout (ko) and seven wild-type patches. Two-sample *t* test comparisons made between stimulation conditions on the same background, and between genetic backgrounds, gave *P* values between 0.35 and 0.92. The rest condition consisted of 188 wild-type (wt) and 100 ko events, and the depolarized condition 228 wt and 60 ko events. The number of events per patch ranged from 32 to 99 for wt and from 10 to 50 for ko.

common to IHC active zones. This relationship is maintained under different experimental conditions, suggesting that release from IHCs is predominantly univesicular. The findings are consistent with numerous studies that measured C_m changes with the cell-attached method and reported that the amount of membrane added per fusion event correlated with the morphological size of secretory vesicles expressed in each of the cell types (13–15, 21, 24). Since this represents one of a few on-cell C_m studies to measure small vesicle fusion events, we start by comparing our findings to those studies and then discuss our results in the context of hair cell synaptic transmission.

The study by He et al. (13) first reported that individual C_m fusion events measured at the synaptic face of the calyx of Held nerve terminal yielded steps of ~73 aF, close to what could be expected for the fusion of single SVs averaging 45 nm in diameter. They later showed that when the cells were depolarized by elevating extracellular KCl (50–100 mM) such that a greater proportion of large “compound” vesicles appeared in the electron micrographs, the outcome was a direct increase in the percentage of larger fusion events (16). This study points to a plasticity in vesicle biogenesis upstream of exocytosis. In a different study that focused on release from posterior pituitary nerve terminals, Klyachko and Jackson (15) showed that C_m fusion event amplitudes were bimodally distributed with peaks at 67 and 412 aF, which corresponds to the size of synaptic-like microvesicles and granules expressed in these cells (vesicle diameters of 48.5 and 125 nm, respectively). The fusion step size distribution remained bimodal at rest when event frequency was ~0.1 Hz, and during high KCl stimulation when event frequency increased to ~0.5 Hz. For comparison, we directly depolarized the patch of membrane relative to the ground electrode and witnessed an elevated event frequency (0.45 Hz), and the outcome was steps of ~40 aF, closely corresponding to SVs with diameters of 36 nm. In total, these studies argue against MVR release being coordinated at the plasma membrane and instead suggest that the amplitudes of fusion events reflect the distribution of SV sizes.

There are potential drawbacks associated with on-cell C_m measurements. One concern is that when the rate of events is kept low so that individual events are well separated, not overlapping, this may preclude an MVR process. However, coordinated MVR does not rely on the random superposition of events and therefore absolute release frequency is not a prerequisite (3). What is more difficult to rule out is whether the on-cell configuration perturbs a mechanism that coordinates SV fusion. As highlighted above, the patches of membrane do exhibit functional behavior; therefore, we favor the view that the recordings reflect presynaptic physiology.

So, how can UVR account for the amplitude diversity of sEPSCs in IHCs? Previous studies using amperometry to measure the amount of transmitter released per fusion event have

shown a strong correlation between quantal size and vesicle volume (35, 42–44). However, when making recordings from the postsynapse, it is difficult to know how much transmitter is released per EPSC since synaptic structure and receptor properties codetermine the response (for review, see refs. 41 and 45). Nonetheless, the amount of transmitter released per SV is thought to have the greatest influence on miniature EPSC (mEPSC) amplitude variance (16, 34, 40, 46). Bekkers et al. (34) put forth the argument that variance in SV volume directly impacts quantal variance and, in doing so, contributes to mEPSC variance. A detailed modeling study on the topic concluded that SV diameters with a CV = 0.2 would yield mEPSC amplitudes with a CV = 0.61 (see table 1 in ref. 36). After removing the largest 6% of the C_m fusion events measured here, the equivalent SV volumes have a CV > 0.6 (CV for equivalent diameter: 0.21), which exceeds the variance associated with K⁺ evoked EPSCs measured from 3-wk-old wild-type mice that were reported to consist mostly of monophasic EPSCs (>92% of the events) with a CV ~0.33 (37). Hence, the variance in the size of fusing SVs is more than enough to account for variance in EPSCs measured from 3-wk-old mice.

It is known that IHC-SGN synaptic structure is refined during development. This is accompanied by more efficient secretion coupling (47), and the EPSCs change significantly through development. Earlier studies examined the influence of development on EPSCs in young rats [postnatal day (P)7 to P21] and found that with age the monophasic EPSCs became more frequent (going from 59 to ~72%), developed faster waveform kinetics, and were shifted to larger amplitudes, which created an unusual skew toward small events (3, 10). Likewise, prehearing mice, P9 to P11, show significant variance in EPSC waveform: ~60% monophasic and 40% multiphasic, and the amplitude distributions for either type of waveform are heavily skewed toward larger events (38), while 3-wk-old mice are almost entirely monophasic (37). It is worth noting that EPSCs measured from mature bullfrog auditory hair cells are exclusively monophasic (39). mEPSCs measured from calyx of Held are monophasic and they to show an age-dependent enhancement in mEPSC amplitude and an acceleration in waveform kinetics through development (48). These age-related changes are widely viewed as improving signaling efficiency (10, 49), but as to how this is achieved is less clear at the IHC-SGN synapse. In the context of a UVR process, the multiphasic events witnessed in young mice may reflect release through a dynamic fusion pore (9), or possibly other presynaptic and postsynaptic changes yet to be identified. However, within the set of monophasic EPSCs, the developmental changes match what has been described for partial receptor saturation under a UVR (see figure 8 in ref. 50), and a common feature associated with saturation is a reduction in variance and a skew toward smaller events (for review, see ref. 45). Partial saturation of IHC-SGN receptors could dampen amplitude variance and potentially explain why variance in SV volume exceeds the variability in EPSC amplitude.

Is there sufficient glutamate in a quantum to support signaling through a UVR process? Franks et al. (36) modeled different presynaptic and postsynaptic arrangements for a simple central synapse, and 2,000–3,000 molecules of glutamate released per SV was sufficient to yield realistic outcomes for UVR. A similar number of glutamate molecules was found to be adequate to model UVR at the IHC-SGN synapse (9). The latter study explored two separate AMPA receptor kinetic schemes, both of which were able to yield ~120–240 pA EPSCs when the quantum equaled 3,000 molecules. This EPSC amplitude approximates what has been measured in 3-wk-old mice. Packing 3,000 glutamate molecules into a 37-nm diameter SV would yield an intravesicular concentration of ~200 mM glutamate. Biochemical (51) and physiological (48) studies suggest that this amount of glutamate in an SV is reasonable, and other neurotransmitter systems are believed to concentrate transmitters in SVs to 100–300 mM (35, 52, 53).

Since a spontaneous EPSC can effectively trigger an SGN-AP (5), and if UVR prevails at this synapse as suggested here and earlier (9), then single SV fusion events should be sufficient to drive SGN spiking. To our knowledge, this level of efficiency, 1 SV to 1 AP, is unprecedented. Interestingly a single hippocampal mossy fiber-CA3 synaptic contact is capable of driving APs, similar to a IHC-afferent contact, yet the quantal content underlying the MF release remains unknown (54). It may seem odd that a ribbon-type AZ would have so many SVs, but only utilize them one at a time. However, a 1 SV to 1 AP ratio is maximally efficient, and this will help IHCs maintain high rates of continual release by mitigating the onset of presynaptic fatigue and reduce the metabolic burden of excess glutamate recycling.

- Robertson D, Paki B (2002) Role of L-type Ca²⁺ channels in transmitter release from mammalian inner hair cells. II. Single-neuron activity. *J Neurophysiol* 87:2734–2740.
- Neef J, et al. (2009) The Ca²⁺ channel subunit beta2 regulates Ca²⁺ channel abundance and function in inner hair cells and is required for hearing. *J Neurosci* 29:10730–10740.
- Glowatzki E, Fuchs PA (2002) Transmitter release at the hair cell ribbon synapse. *Nat Neurosci* 5:147–154.
- Platzter J, et al. (2000) Congenital deafness and sinoatrial node dysfunction in mice lacking class D L-type Ca²⁺ channels. *Cell* 102:89–97.
- Rutherford MA, Chapochnikov NM, Moser T (2012) Spike encoding of neurotransmitter release timing by spiral ganglion neurons of the cochlea. *J Neurosci* 32:4773–4789.
- Kavalali ET (2015) The mechanisms and functions of spontaneous neurotransmitter release. *Nat Rev Neurosci* 16:5–16.
- Vyleta NP, Smith SM (2011) Spontaneous glutamate release is independent of calcium influx and tonically activated by the calcium-sensing receptor. *J Neurosci* 31:4593–4606.
- Rudolph S, Tsai MC, von Gersdorff H, Wadiche JI (2015) The ubiquitous nature of multivesicular release. *Trends Neurosci* 38:428–438.
- Chapochnikov NM, et al. (2014) Uniquantal release through a dynamic fusion pore is a candidate mechanism of hair cell exocytosis. *Neuron* 83:1389–1403.
- Grant L, Yi E, Glowatzki E (2010) Two modes of release shape the postsynaptic response at the inner hair cell ribbon synapse. *J Neurosci* 30:4210–4220.
- Khimich D, et al. (2005) Hair cell synaptic ribbons are essential for synchronous auditory signalling. *Nature* 434:889–894.
- Goutman JD, Glowatzki E (2007) Time course and calcium dependence of transmitter release at a single ribbon synapse. *Proc Natl Acad Sci USA* 104:16341–16346.
- He L, Wu XS, Mohan R, Wu LG (2006) Two modes of fusion pore opening revealed by cell-attached recordings at a synapse. *Nature* 444:102–105.
- Neher E, Marty A (1982) Discrete changes of cell membrane capacitance observed under conditions of enhanced secretion in bovine adrenal chromaffin cells. *Proc Natl Acad Sci USA* 79:6712–6716.
- Klyachko VA, Jackson MB (2002) Capacitance steps and fusion pores of small and large-dense-core vesicles in nerve terminals. *Nature* 418:89–92.
- He L, et al. (2009) Compound vesicle fusion increases quantal size and potentiates synaptic transmission. *Nature* 459:93–97.
- Lollike K, Lindau M, Calafat J, Borregaard N (2002) Compound exocytosis of granules in human neutrophils. *J Leukoc Biol* 71:973–980.
- Meyer AC, et al. (2009) Tuning of synapse number, structure and function in the cochlea. *Nat Neurosci* 12:444–453.
- Sakmann B, Neher E (2009) *Single-Channel Recording* (Springer, New York), 2nd Ed, pp 637–650.
- Dernick G, Gong LW, Tabares L, Alvarez de Toledo G, Lindau M (2005) Patch amperometry: High-resolution measurements of single-vesicle fusion and release. *Nat Methods* 2:699–708.
- Albillos A, et al. (1997) The exocytotic event in chromaffin cells revealed by patch amperometry. *Nature* 389:509–512.
- Lollike K, Borregaard N, Lindau M (1998) Capacitance flickers and pseudoflickers of small granules, measured in the cell-attached configuration. *Biophys J* 75:53–59.
- Henkel AW, Meiri H, Horstmann H, Lindau M, Almers W (2000) Rhythmic opening and closing of vesicles during constitutive exo- and endocytosis in chromaffin cells. *EMBO J* 19:84–93.
- Vardjan N, Stenovc M, Jorgacevski J, Kreft M, Zorec R (2007) Subnanometer fusion pores in spontaneous exocytosis of peptidergic vesicles. *J Neurosci* 27:4737–4746.
- Alés E, et al. (1999) High calcium concentrations shift the mode of exocytosis to the kiss-and-run mechanism. *Nat Cell Biol* 1:40–44.
- Lindau M (2012) High resolution electrophysiological techniques for the study of calcium-activated exocytosis. *Biochim Biophys Acta* 1820:1234–1242.
- Jorgacevski J, et al. (2010) Fusion pore stability of peptidergic vesicles. *Mol Membr Biol* 27:65–80.
- Spruce AE, Breckenridge LJ, Lee AK, Almers W (1990) Properties of the fusion pore that forms during exocytosis of a mast cell secretory vesicle. *Neuron* 4:643–654.
- Debus K, Lindau M (2000) Resolution of patch capacitance recordings and of fusion pore conductances in small vesicles. *Biophys J* 78:2983–2997.
- Johnson SL, Beurg M, Marcotti W, Fettiplace R (2011) Prestin-driven cochlear amplification is not limited by the outer hair cell membrane time constant. *Neuron* 70:1143–1154.
- Guček A, et al. (2016) Dominant negative SNARE peptides stabilize the fusion pore in a narrow, release-unproductive state. *Cell Mol Life Sci* 73:3719–3731.
- Brandt A, Striessnig J, Moser T (2003) Ca_v1.3 channels are essential for development and presynaptic activity of cochlear inner hair cells. *J Neurosci* 23:10832–10840.
- Neef A, et al. (2007) Probing the mechanism of exocytosis at the hair cell ribbon synapse. *J Neurosci* 27:12933–12944.
- Bekkers JM, Richerson GB, Stevens CF (1990) Origin of variability in quantal size in cultured hippocampal neurons and hippocampal slices. *Proc Natl Acad Sci USA* 87:5359–5362.
- Bruns D, Jahn R (1995) Real-time measurement of transmitter release from single synaptic vesicles. *Nature* 377:62–65.
- Franks KM, Stevens CF, Sejnowski TJ (2003) Independent sources of quantal variability at single glutamatergic synapses. *J Neurosci* 23:3186–3195.
- Becker L, et al. (2018) The presynaptic ribbon maintains vesicle populations at the hair cell afferent fiber synapse. *eLife* 7:e30241.
- Jing Z, et al. (2013) Disruption of the presynaptic cytomatrix protein bassoon degrades ribbon anchorage, multiquantal release, and sound encoding at the hair cell afferent synapse. *J Neurosci* 33:4456–4467.
- Li GL, Keen E, Andor-Ardó D, Hudspeth AJ, von Gersdorff H (2009) The unitary event underlying multiquantal EPSCs at a hair cell's ribbon synapse. *J Neurosci* 29:7558–7568.
- Karunanithi S, Marin L, Wong K, Atwood HL (2002) Quantal size and variation determined by vesicle size in normal and mutant *Drosophila* glutamatergic synapses. *J Neurosci* 22:10267–10276.
- Lisman JE, Raghavachari S, Tsien RW (2007) The sequence of events that underlie quantal transmission at central glutamatergic synapses. *Nat Rev Neurosci* 8:597–609.
- Gong LW, Hafez I, Alvarez de Toledo G, Lindau M (2003) Secretory vesicles membrane area is regulated in tandem with quantal size in chromaffin cells. *J Neurosci* 23:7917–7921.
- Moser T, Neher E (1997) Estimation of mean exocytic vesicle capacitance in mouse adrenal chromaffin cells. *Proc Natl Acad Sci USA* 94:6735–6740.
- Grabner CP, Price SD, Lysakowski A, Fox AP (2005) Mouse chromaffin cells have two populations of dense core vesicles. *J Neurophysiol* 94:2093–2104.
- Atwood HL, Karunanithi S (2002) Diversification of synaptic strength: Presynaptic elements. *Nat Rev Neurosci* 3:497–516.
- Wu XS, et al. (2007) The origin of quantal size variation: Vesicular glutamate concentration plays a significant role. *J Neurosci* 27:3046–3056.
- Wong AB, et al. (2014) Developmental refinement of hair cell synapses tightens the coupling of Ca²⁺ influx to exocytosis. *EMBO J* 33:247–264.
- Yamashita T, Ishikawa T, Takahashi T (2003) Developmental increase in vesicular glutamate content does not cause saturation of AMPA receptors at the calyx of Held synapse. *J Neurosci* 23:3633–3638.
- Taschenberger H, von Gersdorff H (2000) Fine-tuning an auditory synapse for speed and fidelity: Developmental changes in presynaptic waveform, EPSC kinetics, and synaptic plasticity. *J Neurosci* 20:9162–9173.
- Malagon G, Miki T, Llano I, Neher E, Marty A (2016) Counting vesicular release events reveals binomial release statistics at single glutamatergic synapses. *J Neurosci* 36:4010–4025.
- Riveros N, Fiedler J, Lagos N, Muñoz C, Orrego F (1986) Glutamate in rat brain cortex synaptic vesicles: Influence of the vesicle isolation procedure. *Brain Res* 386:405–408.
- Kuffler SW, Yoshikami D (1975) The number of transmitter molecules in a quantum: An estimate from iontophoretic application of acetylcholine at the neuromuscular synapse. *J Physiol* 251:465–482.
- Pothos EN, Davila V, Sulzer D (1998) Presynaptic recording of quanta from midbrain dopamine neurons and modulation of the quantal size. *J Neurosci* 18:4106–4118.
- Vyleta NP, Borges-Merjane C, Jonas P (2016) Plasticity-dependent, full detonation at hippocampal mossy fiber-CA3 pyramidal neuron synapses. *eLife* 5:e17977.

Methods

The animals were under the care of the Max Planck Institute for Biophysical Chemistry. The apical coil of cochlea from male and female mice 4–8 wk old were used. Mice were maintained on a C57BL6/J background with/without Ca_v1.3 knockout (4, 32). Control mice were either wild type (+/+) or heterozygous (+/-) for the wild-type Ca_v1.3 gene, and the knockouts were homozygous (-/-). For further details on electrophysiological methods, see *SI Appendix, Methods*.

ACKNOWLEDGMENTS. We thank Profs. Erwin Neher and Manfred Lindau for their expert help on the instrumentation, software, and discussions over the data; Dr. Valeria Zampini who shared her expertise on cell-attached recordings from IHCs with us; and Dr. Jakob Neef for critical feedback on the manuscript. This work was supported by the Max Planck Society and the DFG through the Leibniz program.